applied optics

All acousto-optic modulator laser system for a 12 m fountain-type dual-species atom interferometer

Chuan He,[1,2] Sitong Yan,[1,2] Lin Zhou,[1,*] Sachin Barthwal,[3] Rundong Xu,[1,2] Chao Zhou,[1] Yuhang Ji,[1] Qi Wang,[1,2] Zhuo Hou,[1,2] Jin Wang,[1] and Mingsheng Zhan[1,4]

[1]State Key Laboratory of Magnetic Resonance and Atomic and Molecular Physics, Wuhan Institute of Physics and Mathematics, Innovation Academy for Precision Measurement Science and Technology, Chinese Academy of Sciences, Wuhan 430071, China
[2]School of Physical Sciences, University of Chinese Academy of Sciences, Beijing 100049, China
[3]Light and Matter Physics, Raman Research Institute, Sadashivanagar, Bangalore 560080, India
[4]e-mail: mszhan@wpim.ac.cn
*Corresponding author: lzhou@wpim.ac.cn

Received 26 April 2021; revised 24 May 2021; accepted 24 May 2021; posted 26 May 2021 (Doc. ID 429965); published 10 June 2021

We design and implement a laser system for ^{85}Rb and ^{87}Rb dual-species atom interferometers based on acousto-optic frequency shift and tapered amplifier laser technologies. We use eight-pass acousto-optic modulators to generate repumping lasers for ^{85}Rb and ^{87}Rb atoms. The maximum frequency shift of the laser is 2.8 GHz, and the diffraction efficiency is higher than 20%. We use high-frequency acousto-optic modulators to generate the Raman lasers. This laser system uses only two seed lasers to provide the various frequencies required by ^{85}Rb and ^{87}Rb dual-species atom interferometers, which greatly improves laser usage. The laser system is applied in the equivalence principle test experiment using an ^{85}Rb and ^{87}Rb dual-species atom interferometer. The signal of atoms launched to 12 meters is successfully observed, and the resolution of gravity differential measurement is improved from 8×10^{-9} g to 1×10^{-10} g.

https://doi.org/10.1364/AO.429965

1. INTRODUCTION

Atom interferometers have been widely used in precision measurement of inertial physical parameters, such as gravity [1–3], gravity gradient [4,5], and rotation [6,7]. They have also been used in the measurement of physical constants [8–13] and the test of fundamental physical laws [14–21]. A laser system plays a key role in atom-interferometer-based precision measurement experiments. To improve the measurement precision, the requirements for laser systems in atom interferometers are getting higher. The high-precision equivalence principle test [18,21], for example, requires simultaneous and continuous measurement using a dual-species atom interferometer, and its laser system can provide multiple frequencies. Normally, the frequency spectrum of an independent frequency-stabilized laser is pure, and its frequency tuning range is large. We can use many independent frequency-locked lasers to provide lasers with different frequencies for atom interferometers, especially for non-isotopic dual-species atom interferometers. For example, the rubidium–potassium dual-species atom interferometer needs lasers with wavelengths of 780 nm and 767 nm [17]. However, during a long-term (hours to days, or even longer) continuous measurement, the interruption caused by the lockout of lasers is an important factor affecting the long-term reliable operation of the experiment. Although it is not difficult for a single laser to operate continuously for several days, when there are many such lasers in the laser system, the risk of lockout is greatly increased. Therefore, reducing the number of lasers is an effective way to reduce the uncertainty. For lasers with a frequency difference of less than 10 GHz, frequency shift can be used to reduce the number of lasers. Bonnin *et al.* used fiber electro-optic modulators (EOMs) to generate cooling and repumping lasers for a ^{85}Rb and ^{87}Rb dual-species atom interferometer [22], and this scheme minimized the number of independent lasers. However, the EOM produces many redundant sidebands, which decreases the efficiency of laser usage (the efficiency of the first-order sideband is 34%), and induces unnecessary transitions. Using EOM to realize Raman lasers may also introduce systematic errors, such as an AC Stark shift [23]. Johnson *et al*. applied the serrodyne modulation technique to the fiber phase modulator to increase the efficiency of the sideband laser to >60% [24], and the frequency shift range was from 200 MHz to 1.2 GHz. This method significantly improved the laser usage efficiency. There are, however, still stray sidebands.

Acousto-optic modulator (AOM) is another kind of laser frequency shift device. In general, when the center frequency

of an AOM is on the order of 100 MHz, the diffraction efficiency is high and the frequency components are pure. However, the diffraction efficiency and damage threshold of an AOM will rapidly decrease as the center frequency increases. The diffraction efficiency of a 4.6 GHz high-frequency AOM is only 0.04%, and the output diffracted light is relatively weak. It requires injection locking and other methods to amplify the laser power before it can be used in experiments [25]. Using a 1.5 GHz high-frequency AOM or multipass acousto-optic frequency shift technology to produce a ±1 level sideband, the laser amplified by the cone amplifier can be used as the Raman laser of the ^{85}Rb atom interferometer [26]. However, when preparing lasers for cooling and pumping back ^{85}Rb atoms, this method requires more lasers because the frequency-locking point of the seed laser is far from the resonance frequency. For example, in the potassium atom cooling experiment [27], multipass acousto-optic frequency shift technology was used, and the single-stage sideband frequency shifted to 1.6 GHz. For the laser system of the ^{85}Rb and ^{87}Rb dual-species atom interferometer, the single-sideband must be shifted over 3 GHz. Although the AOM frequency shift scheme has no spurious sidebands, for the ^{85}Rb and ^{87}Rb dual-species atom interferometers, large-scale frequency shifting and high-efficiency diffraction generation laser beams of various frequencies are still very challenging.

Here, we design and implement a laser system for the ^{85}Rb and ^{87}Rb dual-species atom interferometer based on AOMs and taper amplifier technology. We use a 350 MHz AOM and eight-pass acousto-optic frequency shift technology to achieve a laser output with a diffraction efficiency of 20%, frequency shift of 2.8 GHz, and power greater than 30 mW. We obtain seven sets of different lasers with the frequency difference between 1.1 and 3.8 GHz required by the ^{85}Rb and ^{87}Rb dual-species atom interferometer with only two seed lasers. Compared to similar jobs, our ^{85}Rb and ^{87}Rb laser systems have higher laser usage efficiency and better reliability. We combine the fiber EOM high-order sideband frequency locking [28], laser time-division multiplexing [29], laser spectrum quality analysis [30], and other technologies developed in the early stage to apply this laser system to the atom interferometer equivalence principle test experiment. The atomic fountain signal is realized up to 12 m, and the resolution of the dual-species atomic interference gravity differential measurement is improved from 8×10^{-9} g [18] to 1×10^{-10} g.

2. EXPERIMENTAL DESIGN

The energy level of D_2 lines of ^{85}Rb and ^{87}Rb atoms and their lasers for atom interferometers are shown in Fig. 1. The frequency difference between the cooling lasers of ^{85}Rb and ^{87}Rb, repumping lasers of ^{85}Rb and ^{87}Rb required are 1.13 GHz, 2.90 GHz, and 2.54 GHz respectively as shown in Fig. 1 (b). The frequencies of the corresponding probe and blow-away lasers are similar to the cooling lasers called the cooling laser group. The four waves double Raman diffraction (FWDR) atom interference scheme requires a pair of chirped lasers ω_1 and ω_2 with a mini frequency difference. This pair of lasers together with ω_3 are double-diffraction Raman lasers for ^{85}Rb atoms, and ω_1, ω_2, and ω_4 are double-diffraction Raman lasers for ^{87}Rb atoms. The frequency difference between ω_1, ω_3, and ω_4 are 3.03 GHz and 3.80 GHz. The lasers with frequencies of ω_1, ω_2, ω_3, and ω_4 are called the Raman laser group.

To optimize the dual-species atom interference experiment, the above seven sets of lasers with a frequency difference at GHz level need to be amplified by tapered amplifiers (TAs). The TAs with an output power of 1−2W generally require 10−30 mW seed lasers. For a laser system of a ^{85}Rb and ^{87}Rb dual-species atom interferometer, the biggest challenge in adopting the AOM shift scheme is not only to realize the required laser with various frequencies but also to output laser power that is large enough to meet the requirement of the incident seed laser for TAs. To solve this problem, we design an eight-pass acousto-optic shift (AOS) system for the cooling laser group and design a high-frequency AOM with low phase noise and injection locking for the Raman laser group.

A. Cooling Laser Group for Dual-Species Atoms

1. Design of the Cooling Laser Group

We use two double-pass AOMs to, respectively, generate cooling lasers with a frequency difference of 1.126 GHz for ^{85}Rb and ^{87}Rb atoms and use an eight-pass AOS scheme to achieve the repumping lasers with a frequency shift of 2.8 GHz and a

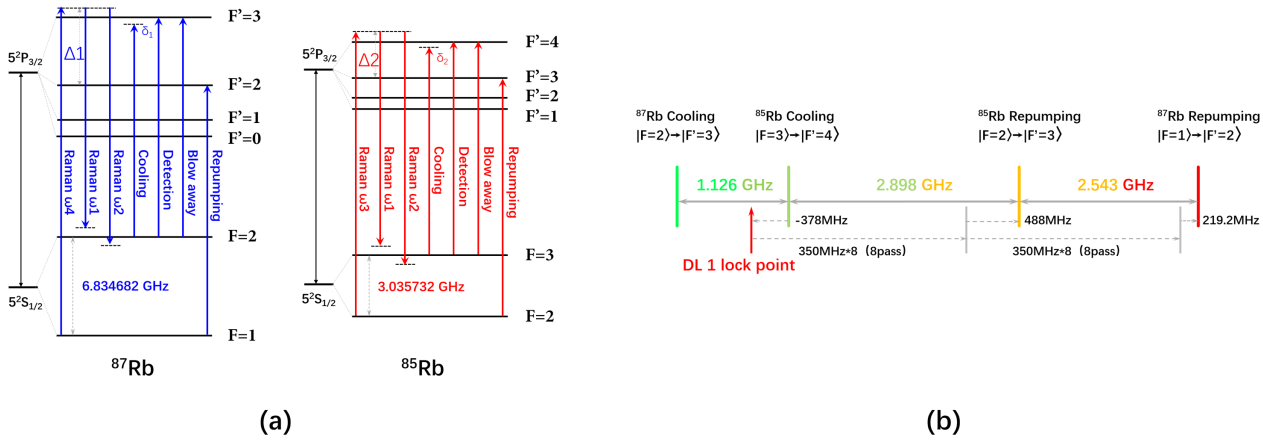

Fig. 1. Energy level and frequency relationship. (a) Energy level of D_2 lines of ^{87}Rb and ^{85}Rb atoms. δ_1 and δ_2 are detunings of cooling lasers for ^{87}Rb and ^{85}Rb atoms, Δ_1 and Δ_2 are detunings of their Raman lasers. (b) Frequency relationship of cooling laser group.

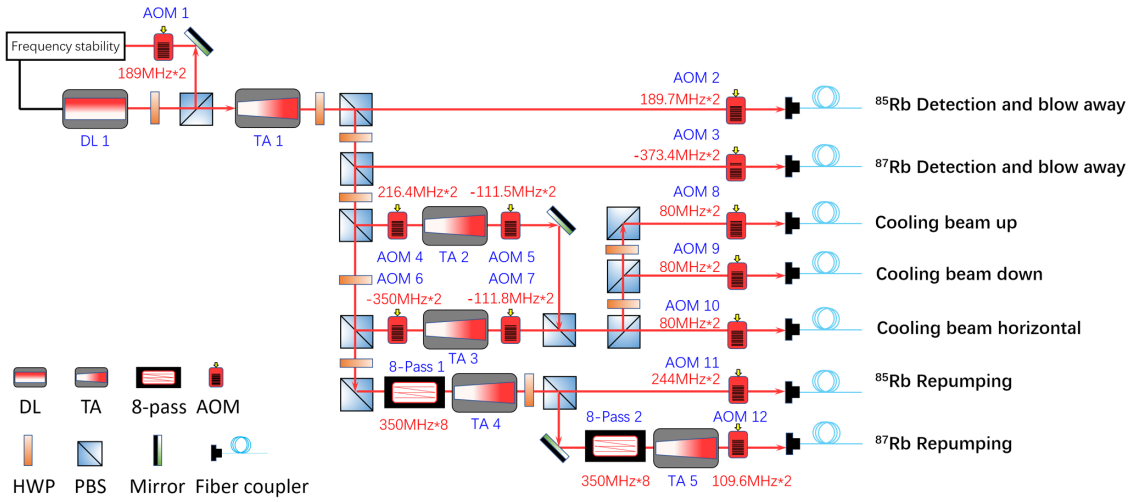

Fig. 2. Schematic diagram of cooling laser group. The system consists of a diode laser (DL) and five tapered amplifiers (TAs). All laser frequency shifts are achieved through AOMs.

diffraction efficiency of 20%. This scheme requires only one seed laser to obtain a pure and high-power cooling laser group for ^{85}Rb and ^{87}Rb dual-species atoms. The schematic diagram of this scheme is shown in Fig. 2.

The cooling laser group includes a diode laser (DL) and five TAs. The seed laser output by a DL 1 is injected into TA 1 for power amplification. The output laser of TA 1 is divided into several ways and frequency shifted by AOMs. The cooling seed lasers for ^{85}Rb and ^{87}Rb atoms are injected into TA 2 and TA 3, respectively, and the repumping seed laser for ^{85}Rb atoms is injected into TA 4. The repumping seed laser for ^{87}Rb atoms is obtained from that of ^{85}Rb by frequency shifting. Except for the two AOMs used to generate the repumping seed lasers, the remaining 12 AOMs are all a double-pass configuration.

The seed laser output by DL 1 is shifted 378 MHz by AOM 1 and used for polarization spectrum frequency stabilization, where it is locked on the transition of ^{85}Rb$|F = 3\rangle - |F' = 4\rangle$. The frequency difference between the seed laser and the transition ^{85}Rb$|F = 3\rangle - |F' = 4\rangle$ is 378 MHz, and the linewidth of the laser is on the order of 100 kHz. The seed laser is amplified to 1.5 W by TA 1 and then split into several paths. Two of them are shifted 379.4 MHz and −746.8 MHz by two AOMs (AOM 2 and AOM 3) and used for the detection and blow-away lasers for ^{85}Rb and ^{87}Rb, respectively.

The cooling seed lasers for ^{85}Rb and ^{87}Rb atoms are shifted 432.8 MHz and −700 MHz by AOM 4 and AOM 6, respectively, and then they are amplified to 1.5 W by TA 2 and TA 3. Two lasers output from the two TAs are shifted −220 MHz by two 110 MHz AOMs (AOM 5 and AOM 7), and then they are combined and coupled into one optical fiber. The frequencies of cooling lasers for ^{85}Rb and ^{87}Rb atoms are independently controlled by AOM 5 and AOM 7, to meet the need for frequency tuning and intensity control of the lasers in the polarization gradient cooling (PGC) process. The solution above can realize the overall frequency and intensity control of the cooling laser group so that the frequency and power tuning of the three pairs of oppositely propagating cooling lasers are kept relatively consistent, and the implementation of the PGC process is ensured.

The three laser beams output from the optical fiber are then shifted 160 MHz by three 80 MHz AOMs (AOM 8, AOM 9, and AOM 10), respectively. They are used for a 3D magneto-optical trap (3D-MOT). In the launching process of the atom fountain, the lasers for moving molasses must maintain a certain frequency difference in the launching direction. Our 3D-MOT uses a (0, 0, 1) configuration with two pairs of horizontal lasers and one pair of vertical lasers; therefore, the frequencies of the vertical laser pair must be tuned. We use three independent AOMs for cooling lasers for 3D-MOT to meet the need to frequency tune moving molasses.

The generation process of repumping seed laser for ^{85}Rb and ^{87}Rb atoms is as follows: A 300 mW laser beam was shifted 2.8 GHz by the first eight-pass AOS system; then it was amplified by TA 4. A part of the output from TA 4 is shifted 488 MHz by AOM 11 as the repumping laser of ^{85}Rb atoms. The other part is shifted 2.8 GHz again by the second eight-pass AOS system and enters TA 5 for power amplification. The laser output from TA 5 is shifted 219.2 MHz by AOM 12 as the repumping laser of ^{87}Rb atoms.

In the cooling laser group, the frequencies of all lasers maintain very good relative stability with the seed laser. The relative frequency difference is measured to be less than 10 Hz by the beat method. This solution provides enough lasers for the preparation and detection process of ^{85}Rb and ^{87}Rb dual-species atoms. As long as the seed DL 1 is locked, the entire cooling laser group can work stably. In addition, this system also has very good scalability. For example, if the linewidth of the seed DL 1 is further narrowed to 10 kHz, the frequency stability of all lasers in the cooling laser group will be improved simultaneously.

2. *Eight-Pass Acousto-Optic Shift System*

We use AOS techniques to provide a reliable laser source solution for the aforementioned complex cooling laser group, which is currently the only all-AOM scheme for the preparation of ^{85}Rb and ^{87}Rb dual-species atom sources. In this scheme, the eight-pass AOS that prepares the repumping seed lasers for ^{85}Rb and ^{87}Rb atoms is the most critical. General multipass AOS has

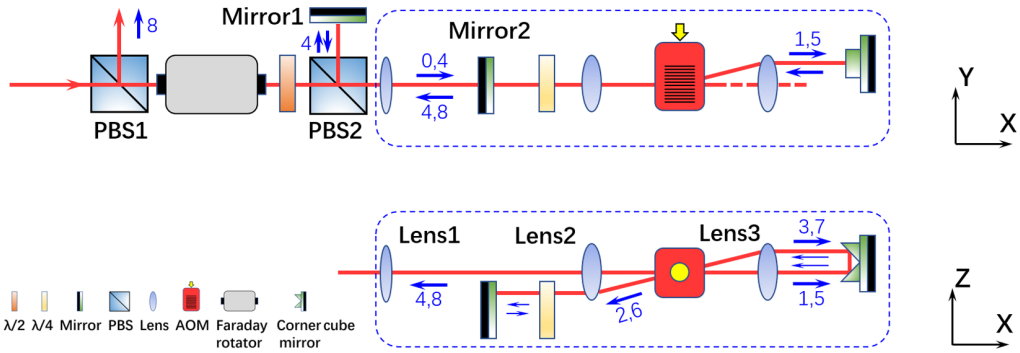

Fig. 3. Schematic diagram of the eight-pass AOS system. Only using a 350 MHz AOM, we can achieve a laser frequency shift up to 3 GHz. The figure above is a top view of the schematic, and the figure below is the front view of the schematic in the dashed box.

been reported before [27,31–33]. Among them, the 12-pass shift system [33] with a frequency shift range of 5 GHz is currently the largest range AOM scheme, but this scheme cannot match the requirements of ^{85}Rb and ^{87}Rb dual-species atom interference experiments. To solve this problem, we designed an eight-pass AOS scheme based on 350 MHz AOMs.

The core of the eight-pass AOS scheme is to combine the polarization characteristics of the laser with the diffraction characteristics of the AOM to achieve the continuous multiple diffractions of the laser, and finally separate it from the laser beam with other unwanted frequency components. Through the combination of the $\lambda/4$ wave plate and the polarization beam splitter (PBS), and the combination of Faraday rotator and PBS, the number of diffractions can be increased by two times. In addition, the horizontally placed AOM is not sensitive to the vertical incident angle of the laser, so we can double the number of laser diffractions by changing the vertical incident angle of the laser to finally achieve and eight-times diffraction. To realize the spatial separation of the diffracted laser beams, we specially designed an external reflection right-angle prism to make the laser beam maintain better linear polarization during the propagation process. In the process of the laser beam passing through the AOM, every time a + 1 order (or −1 order) diffraction occurs, its frequency changes once, and the frequency shift is $f = n \times f_0$, where f_0 is the RF frequency driving the AOM, and n is the number of times the laser has passed through the AOM. In the experiment, we achieve a 6 GHz (3 GHz + 3 GHz) shift by a 350 MHz AOM and eight-pass AOS scheme. This frequency shift range meets the requirement of the repumping laser for ^{85}Rb and ^{87}Rb dual-species atoms (Fig. 1).

The eight-pass AOS process is shown in Fig. 3. First, we compress and collimate the laser beam by a pair of convex lens groups, to achieve an optimal matching of the parameters of the laser and the AOM, so that the first diffraction efficiency of the +1 order (−1 order) laser beam reaches 89%. (NOTE: The "match" here refers to the coincidence of the laser spot and the effective diffraction area of the AOM, as well as the matching of the propagation direction and divergence of the laser beam with the AOM Bragg angle.) After that, the outgoing diffracted laser beam is raised about 2 mm by the outer right-angle prism and then reflected and passes through the AOM again to produce the second diffraction. The second diffraction laser beams are all P-polarized. After the second diffraction laser beam passes through the $\lambda/4$ wave plate, it is reflected by Mirror 2 and passes through the $\lambda/4$ wave plate again. The laser beam returns from the original path and propagates in S polarization and the third and fourth diffraction occurs in sequence. The fourth diffraction beam is still S-polarized, and is reflected when passing through the PBS2, and Mirror 1 reflects the laser beam to the original path again. The reflected laser beam sequentially passes through the AOM and undergoes the fifth–eighth diffractions, where the fifth and sixth diffraction beams are S-polarized, and the seventh and eighth diffraction beams are P-polarized. After the laser beam output of the eighth diffraction passes through the Faraday rotator, the linear polarization direction is changed by 90° relative to the laser beam before entering the AOM. Therefore, it is reflected when passing through PBS1; thus, the laser beams are separated. Through the process above, we have realized an eight-pass AOS system with a frequency shift of 2.8 GHz and a diffraction efficiency of more than 20%.

B. FWDR Raman Laser System

Compared to the cooling laser group, the Raman lasers of an atom interferometer require lower phase noise. Because the structure of the eight-pass AOS is relatively complicated, any small vibration or deformation of the optics can introduce phase noise to the laser beam. Therefore, the eight-pass AOS scheme is not suitable to prepare the Raman laser group. We can use 1.5−1.7 GHz AOMs, which have a low diffractive efficiency but a relatively simple structure to prepare the Raman laser group. In the atom interferometer experiment, a pair of vertical cooling lasers are from different fiber collimators and they are completely overlapped with the Raman lasers in space, but are used at different times. Therefore, it is necessary to carefully design the Raman lasers so that they are helpful to achieve high common-mode rejection in gravity differential measurement using a ^{85}Rb and ^{87}Rb dual-species atom interferometer without specular reflection.

The basic principle of the FWDR method used to test the equivalence principle by dual-species atom interferometer is referred to [18], where the Raman laser group consists of a seed laser and four TAs (as shown in Fig. 4). A part of the laser beam emitted from a DL 2 is shifted −4.5 GHz by a fiber EOM and then used for frequency stabilization by polarization spectrum. The frequency of the DL 2 is locked between the absorption

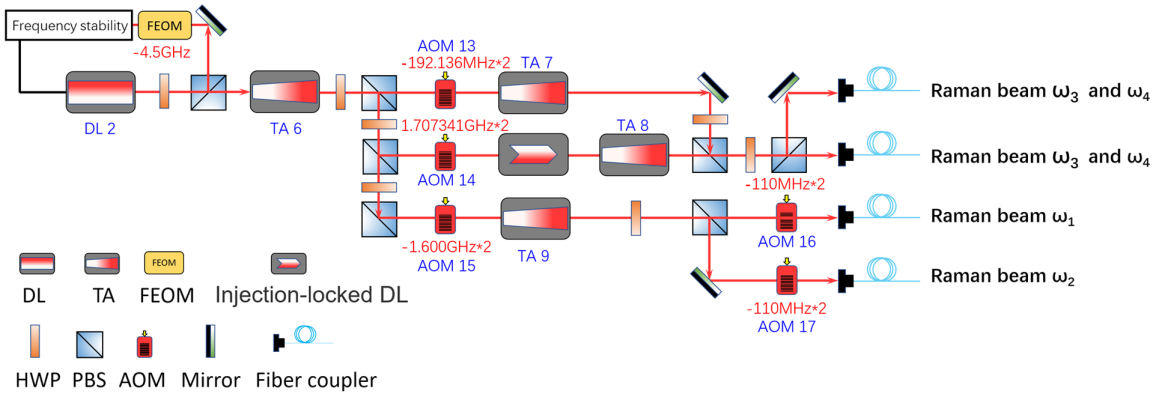

Fig. 4. Experimental schematic of the FWDR Raman laser system. The Raman laser system consists of a DL and four TAs.

peaks ^{85}Rb$|F=2\rangle - |F'=3\rangle$ and ^{87}Rb$|F=1\rangle - |F'=2\rangle$. The remaining laser output from DL 2 enters TA 6 for power amplification, and the output from TA 6 is divided into three beams. The first 300 mW beam is shifted −3.2 GHz by a 1.5 GHz high-frequency AOM (AOM 15) and then used as a 16 mW seed laser. The seed laser is amplified by TA 9 and then passes through two 110 MHz AOMs (AOM 16 and AOM 17) to generate chirped lasers ω_1 and ω_2. The second 100 mW beam is shifted −384 GHz by AOM 13 and amplified by TA 7 to generate ω_3. The third 50 mW beam is shifted 3.4 GHz by a 1.7 GHz high-frequency AOM (AOM 14) and used as a 1 mW seed laser. After injecting and locking a seed laser, the 1 mW seed laser is amplified to 1.5 W by TA 8. As the ω_4 requires more power, and the diffraction efficiency of the 1.7 GHz AOM (AOM 14) is very low, so we adopted an injection-locked laser scheme.

The gravity differential measurement with a high common-mode rejection ratio is a key to the high-precision test of equivalence principle using a dual-species atom interferometer. In the double-diffraction Raman atom interferometer, non-chirped Raman lasers (ω_3 and ω_4) participate in two transitions processes, and their phase shifts are canceled during the interference process. Therefore, the phase of the FWDR atom interferometer is not sensitive to non-chirped lasers. As long as the dual-species atoms share the chirped lasers, the common-mode suppression of phase noise can be achieved. However, because the non-chirped Raman lasers propagated in opposite directions (ω_3 propagates upward and ω_3 propagates downward), their noise are different and cannot be completely canceled out. Fortunately, the frequency difference between the non-chirped lasers ω_3 and ω_4 for ^{85}Rb and ^{87}Rb atoms is on the order of GHz, when the laser beams propagate synchronously inside the optical fiber, their response difference to the same noise is only about 10^{-6} (the ratio of the laser wave vector difference to the laser absolute wave vector). Therefore, we combine the ω_3 and ω_4 laser beams after power amplification, and then divide them into two groups with the same polarization, and couple them into the fiber for upward and downward transmission, respectively. As shown in Fig. 5, the Raman laser system and cooling laser system are combined by a laser time-division multiplexing system, but they are used at different times. Although this design cannot completely suppress the influence of laser transmission noise on the absolute phase shift, it can reduce its influence on the relative phase shift difference of the

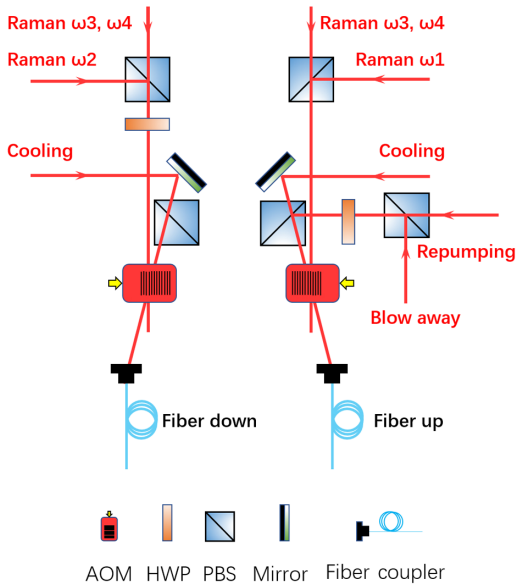

Fig. 5. Experimental schematic of the laser time-division multiplexing system. Raman laser system and cooling laser system are combined by the laser time-division multiplexing system.

dual-species atom interferometer by six orders of magnitude. In the experiment, even though the atom interference fringes of $T = 10$ ms cannot be seen by scanning the phase of the lasers, the high-precision gravitational differential measurement of $T = 300$ ms using a dual-species atom interferometer can be still achieved.

The Raman laser system is composed of a frequency-locked seed laser and an injection-locked laser. Through the AOS scheme, we can get a high-power laser with a pure spectrum. In addition, through the special design of the non-chirped laser, we can achieve high-precision gravity differential measurement using a dual-species atom interferometer without specular reflection of the Raman laser. According to our previous research on Raman laser phase noise [34], the phase noise of our laser system will be worse than that with feedback. But the Raman laser system satisfies our current experimental needs.

3. EXPERIMENTAL RESULTS

A. Performance of the Multipass Acousto-Optic Frequency Shift

We now test the performance of the eight-pass AOS system. By changing the frequency and power of the RF drive signal of the AOM, the dependence of the first, second, fourth, and eighth diffracted laser beams on the RF frequency and power are investigated, respectively. The relationship between laser diffraction efficiency and RF frequency is shown in Fig. 6, where, η $(\eta = P_{in}/P_{out})$ represents the diffraction efficiency of the AOM, P_{in} is the incident laser power of the AOM, and P_{out} is the diffracted laser power of the AOM. In the eight-pass AOS system, when the laser is diffracted for the first time, its diffraction efficiency near the center frequency is as high as 89%. During the second and fourth diffractions, the highest laser diffraction efficiency also reaches 80% and 64%, respectively. This efficiency is in the n-th power relationship, which also shows that the first four diffraction efficiencies are the same. After completing the eighth diffraction, the diffraction efficiency of the output lasers at the center frequency of the AOM can reach 22%, which deviates far from the result of 0.89 to the 8th power. The reasons for this include: The loss of the Faraday rotator is large and, as the number of diffraction increases, the match between the laser and the AOM deteriorates, resulting in a decrease in the diffraction efficiency. The bandwidth of the eight-pass AOS system is about 260 MHz, and the diffraction efficiency exceeds 20% in the center frequency range of 120 MHz.

From the measurement results, it can be seen that after the laser is shifted by 2.8 GHz through the eight-pass AOS system, the diffraction efficiency is higher than 20%, and the damage threshold is greater than 500 mW. Therefore, the power of the output laser of the eight-pass AOS system is much greater than the seed laser power required by the TA. The eight-pass AOS scheme can be further simplified into a four-pass scheme, which also has a reference value for laser cooling of other species atoms.

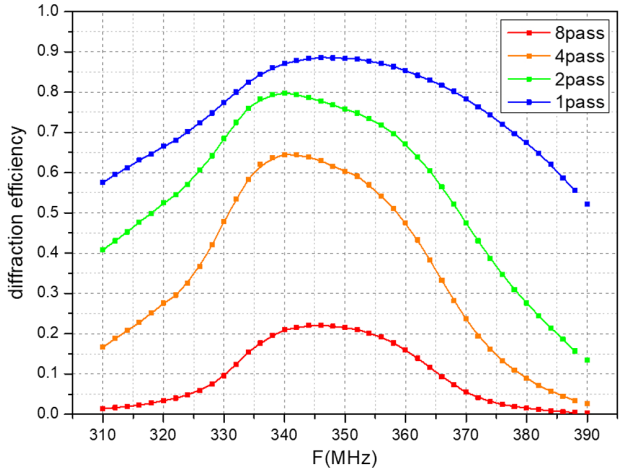

Fig. 6. Frequency dependence of the eight-pass acousto-optic frequency shift system. The center frequency of the AOM is 350 MHz. For the eighth diffraction, the diffraction efficiency of the laser at the center frequency of the AOM can reach 22%.

B. Atom Fountain and Equivalence Principle Test

Our cooling laser group is used to cool and trap ^{85}Rb and ^{87}Rb atoms and realize an atom fountain. The maximum launch height of the atom is 12 m. By optimizing the experimental parameters, we successfully observed the fluorescence signal of the atoms fall from 12 m above.

Figure 7 shows the time-of-flight (TOF) signal of ^{85}Rb atoms after being launched up to different heights. We first prepare 3×10^9 ^{85}Rb atoms through the 3D-MOT, then turn off the magnetic field and realize the vertical launching of the atoms by moving molasses. In the launching process, we need to tune the frequency of the upward cooling laser by δ_c. At the same time, the frequency of the downward cooling laser is tuned $-\delta_c$. The relationship between the initial launching velocity of the atoms and the frequency tuning of the cooling laser pair is expressed as $v_l = \lambda\delta_c$, where λ is the wavelength of the laser. We successively change the tuning frequency of the cooling laser pair in the vertical direction and detected the falling signal after the atoms are launched to different heights.

We also realize gravity differential measurement using a dual-species atom interferometer. We use the Raman laser system to perform coherent operations on the launched atoms [18,34,35], and realize a dual-species Mach–Zehnder atom interferometer by applying Raman pulse sequences $\pi/2 - \pi - \pi/2$ to atoms. In the experiment, the height of the atoms launched is 2.5 m, the duration of the $\pi/2$ pulse is 31 μs, the pulse interval $T = 299.353$ ms, and the single measurement period of the experiment is 3.5 s. The experimental results are shown in Fig. 8. We take the population of ^{85}Rb$|F = 2, m_F = 0\rangle$ state as the x axis, and the population of ^{87}Rb$|F = 1, m_F = 0\rangle$ state as the y axis. For every 40 data, the differential phase shift of the dual-species atom interferometer is obtained by ellipse fitting [36]. As shown in the red data in Fig. 8(b), the Allan deviation after integrating 17920 s is 9.4×10^{-11}.

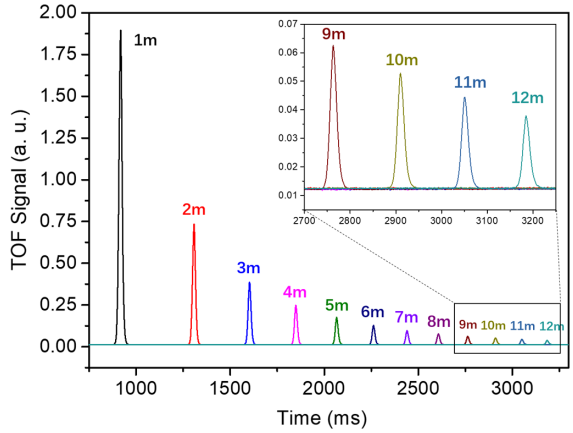

Fig. 7. Time-of-flight (TOF) signal after the atom is launched. The heights are controlled by changing the tuning frequency of the cooling laser pair in the vertical direction, and the falling atoms are detected by laser-induced fluorescence.

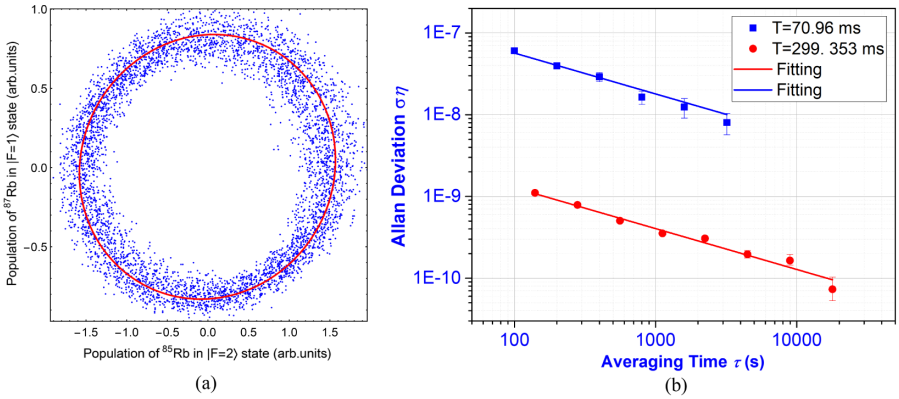

Fig. 8. Differential gravity measurement. (a) Population of ^{87}Rb in $|F = 1\rangle$ state versus population of ^{85}Rb in $|F = 2\rangle$ state. We extract the differential phase of the dual-species interferometer by ellipse fitting. (b) Allan deviation of differential gravity measurement data of ^{85}Rb and ^{87}Rb atoms. The blue data in the figure is from 2015, the deviation of averaging 3200 s is 0.8×10^{-8}. The red data in the figure is from this work. The deviation of averaging 17920 s is 9.4×10^{-11}.

4. DISCUSSION AND CONCLUSION

We designed and implemented an all-AOM optical system for a dual-species atom interferometer. In the cooling laser group, the eight-pass AOS technique enables the laser frequency shift to 2.8 GHz and still achieves a diffraction efficiency above 20%, which solves the frequency-shifting problem of repumping lasers for ^{85}Rb and ^{87}Rb atoms. In the Raman laser group, the Raman laser is obtained by using the high-frequency AOM. This optical system was applied in the equivalence principle test using a dual-species ^{85}Rb and ^{87}Rb atom interferometer. The falling signal after the atom was launched to 12 meters was successfully observed. After a long-term continuous measurement, the resolution of gravity differential measurement is better than 1×10^{-10} g. This optical system effectively reduces the number of frequency-locked lasers in the experiment and improves the system reliability. We can further improve the diffraction efficiency of the high-frequency AOM, so that the Raman lasers do not need the injection-locked DL. Through AOS technology, the cooling laser and the Raman laser share the same seed laser, making the laser system a single laser source system. It is also possible to further reduce the noise of the Raman laser system through solutions such as phase compensation [34]. We believe this laser system lays the foundation for the high-precision equivalence principle test [18].

Funding. National Key Research and Development Program of China (2016YFA0302002); National Natural Science Foundation of China (11574354, 91536221, 91736311); Strategic Priority Research Program of the Chinese Academy of Sciences (XDB21010100); Youth Innovation Promotion Association of the Chinese Academy of Sciences (2016300).

Disclosures. The authors declare no conflicts of interest.

Data Availability. Data underlying the results presented in this paper are not publicly available at this time but may be obtained from the authors upon reasonable request.

REFERENCES

1. A. Peters, K. Y. Chung, and S. Chu, "Measurement of gravitational acceleration by dropping atoms," Nature **400**, 849–852 (1999).
2. Z. K. Hu, B. L. Sun, X. C. Duan, M. K. Zhou, L. L. Chen, S. Zhan, Q. Z. Zhang, and J. Luo, "Demonstration of an ultrahigh-sensitivity atom-interferometry absolute gravimeter," Phys. Rev. A **88**, 043610 (2013).
3. X. J. Wu, Z. Pagel, B. S. Malek, T. H. Nguyen, F. Zi, D. S. Scheirer, and H. Müller, "Gravity surveys using a mobile atom interferometer," Sci. Adv. **5**, eaax0800 (2019).
4. M. J. Snadden, J. M. McGuirk, P. Bouyer, K. G. Haritos, and M. A. Kasevich, "Measurement of the Earth's gravity gradient with an atom interferometer-based gravity gradiometer," Phys. Rev. Lett. **81**, 971–974 (1998).
5. F. Sorrentino, Q. Bodart, L. Cacciapuoti, Y. H. Lien, M. Prevedelli, G. Rosi, L. Salvi, and G. M. Tino, "Sensitivity limits of a Raman atom interferometer as a gravity gradiometer," Phys. Rev. A **89**, 023607 (2014).
6. B. Canuel, F. Leduc, D. Holleville, A. Gauguet, J. Fils, A. Virdis, A. Clairon, N. Dimarcq, C. J. Bordé, A. Landragin, and P. Bouyer, "Six-axis inertial sensor using cold-atom interferometry," Phys. Rev. Lett. **97**, 010402 (2006).
7. D. S. Durfee, Y. K. Shaham, and M. A. Kasevich, "Long-term stability of an area-reversible atom-interferometer Sagnac gyroscope," Phys. Rev. Lett. **97**, 240801 (2006).
8. J. B. Fixler, G. T. Foster, J. M. McGuirk, and M. A. Kasevich, "Atom interferometer measurement of the Newtonian constant of gravity," Science **315**, 74–77 (2007).
9. G. Rosi, F. Sorrentino, L. Cacciapuoti, M. Prevedelli, and G. M. Tino, "Precision measurement of the Newtonian gravitational constant using cold atoms," Nature **510**, 518–521 (2014).
10. D. S. Weiss, B. C. Young, and S. Chu, "Precision measurement of $\hbar$/m Cs based on photon recoil using laser-cooled atoms and atomic interferometry," Appl. Phys. B **59**, 217–256 (1994).
11. R. Bouchendira, P. Clade, S. Guellati-Khelifa, F. Nez, and F. Biraben, "New determination of the fine structure constant and test of the quantum electrodynamics," Phys. Rev. Lett. **106**, 080801 (2011).
12. R. H. Parker, C. H. Yu, W. C. Zhong, B. Estey, and H. Müller, "Measurement of the fine-structure constant as a test of the Standard Model," Science **360**, 191–195 (2018).
13. L. Morel, Z. Yao, P. Cladé, and S. Guellati-Khélifa, "Determination of the fine-structure constant with an accuracy of 81 parts per trillion," Nature **588**, 61–65 (2020).
14. H. Müller, A. Peters, and S. Chu, "A precision measurement of the gravitational redshift by the interference of matter waves," Nature **463**, 926–929 (2010).
15. S. Fray, C. A. Diez, T. W. Hänsch, and M. Weitz, "Atomic Interferometer with amplitude gratings of light and its applications to atom based tests of the equivalence principle," Phys. Rev. Lett. **93**, 240404 (2004).

16. M. G. Tarallo, T. Mazzoni, N. Poli, D. V. Sutyrin, X. Zhang, and G. M. Tino, "Test of Einstein equivalence principle for 0-spin and half-integer-spin atoms: search for spin-gravity coupling effects," Phys. Rev. Lett. **113**, 023005 (2014).
17. D. Schlippert, J. Hartwig, H. Albers, L. L. Richardson, C. Schubert, A. Roura, W. P. Schleich, W. Ertmer, and E. M. Rasel, "Quantum test of the universality of free fall," Phys. Rev. Lett. **112**, 203002 (2014).
18. L. Zhou, S. T. Long, B. Tang, X. Chen, D. F. Gao, W. C. Peng, W. T. Duan, J. Q. Zhong, Z. Y. Xiong, J. Wang, Y. Z. Zhang, and M. S. Zhan, "Test of equivalence principle at 10^{-8} level by a dual-species double-diffraction Raman atom interferometer," Phys. Rev. Lett. **115**, 013004 (2015).
19. B. Barrett, L. Antoni-Micollier, L. Chichet, B. Battelier, T. Lévèque, A. Landragin, and P. Bouyer, "Dual matter-wave inertial sensors in weightlessness," Nat. Commun. **7**, 13786 (2016).
20. X. C. Duan, M. K. Zhou, X. B. Deng, H. B. Yao, C. G. Shao, J. Luo, and Z. K. Hu, "Test of the universality of free fall with atoms in different spin orientations," Phys. Rev. Lett. **117**, 023001 (2016).
21. P. Asenbaum, C. Overstreet, M. Kim, J. Curti, and M. A. Kasevich, "Atom-interferometric test of the equivalence principle at the 10^{-12} Level," Phys. Rev. Lett. **125**, 191101 (2020).
22. A. Bonnin, N. Zahzam, Y. Bidel, and A. Bresson, "Simultaneous dual-species matter-wave accelerometer," Phys. Rev. A **88**, 043615 (2013).
23. A. Gauguet, T. E. Mehlstäubler, T. Lévèque, J. Le Gouët, W. Chaibi, B. Canuel, A. Clairon, F. P. Dos Santos, and A. Landragin, "Off-resonant Raman transition impact in an atom interferometer," Phys. Rev. A **78**, 043615 (2008).
24. D. M. S. Johnson, J. M. Hogan, S.-W. Chiow, and M. A. Kasevich, "Broadband optical serrodyne frequency shifting," Opt. Lett. **35**, 745–747 (2010).
25. P. Bouyer, T. L. Gustavson, K. G. Haritos, and M. A. Kasevich, "Microwave signal generation with optical injection locking," Opt. Lett. **21**, 1502–1504 (1996).
26. L. Zhou, Z. Y. Xiong, W. Yang, B. Tang, W. C. Peng, Y. B. Wang, P. Xu, J. Wang, and M. S. Zhan, "Measurement of local gravity via a cold atom interferometer," Chin. Phys. Lett. **28**, 013701 (2011).
27. B. Lu and D. J. Wang, "A four-pass acousto-optic modulator system for laser cooling of sodium atoms," Rev. Sci. Instrum. **88**, 076105 (2017).
28. W. C. Peng, L. Zhou, S. T. Long, J. Wang, and M. S. Zhan, "Locking laser frequency of up to 40 GHz offset to a reference with a 10 GHz electro-optic modulator," Opt. Lett. **39**, 2998–3001 (2014).
29. W. Yang, L. Zhou, S. T. Long, W. C. Peng, J. Wang, and M. S. Zhan, "Time-division-multiplexing laser seeded amplification in a tapered amplifier," Chin. Opt. Lett. **13**, 011401 (2015).
30. C. Zhou, S. Barthwal, W. D. Zhang, C. He, B. Tang, L. Zhou, J. Wang, and M. S. Zhan, "Characterization and optimization of a tapered amplifier by its spectra through a long multi-pass rubidium absorption cell," Appl. Opt. **57**, 7427–7434 (2018).
31. E. A. Donley, T. P. Heavner, F. Levi, M. O. Tataw, and S. R. Jefferts, "Double-pass acousto-optic modulator system," Rev. Sci. Instrum. **76**, 063112 (2005).
32. F. B. J. Buchkremer, R. Dumke, C. Buggle, G. Birkl, and W. Ertmer, "Low-cost setup for generation of 3 GHz frequency difference phase-locked laser light," Rev. Sci. Instrum. **71**, 3306–3308 (2000).
33. C. Zhou, C. He, S. T. Yan, Y. H. Ji, L. Zhou, J. Wang, and M. S. Zhan, "Laser frequency shift up to 5 GHz with a high-efficiency 12-pass 350-MHz acousto-optic modulator," Rev. Sci. Instrum. **91**, 033201 (2020).
34. K. Wang, Z. W. Yao, R. B. Li, S. B. Lu, X. Chen, J. Wang, and M. S. Zhan, "Hybrid wide-band, low-phase-noise scheme for Raman lasers in atom interferometry by integrating an acousto-optic modulator and a feedback loop," Appl. Opt. **55**, 989–992 (2016).
35. L. Zhou, C. He, S. T. Yan, X. Chen, W. T. Duan, R. D. Xu, C. Zhou, Y. H. Ji, S. Barthwal, Q. Wang, Z. Hou, Z. Y. Xiong, D. F. Gao, Y. Z. Zhang, W. T. Ni, J. Wang, and M. S. Zhan, "United test of the equivalence principle at 10^{-10} level using mass and internal energy specified atoms," arXiv 1904.07096v2 [quant-ph] (2019).
36. G. T. Foster, J. B. Fixler, J. M. McGuirk, and M. A. Kasevich, "Method of phase extraction between coupled atom interferometers using ellipse-specific fitting," Opt. Lett. **27**, 951–953 (2002).